Results

1. Isolation of two novel aPKC alleles

From the original maternal screen, nine groups were established. Complementation analysis of one of the groups with both the 2R deficiency and lethal p-elements indicated that this group with two alleles was allelic to the DaPKC gene (Table 2). Sequencing and cloning of the affect gene in these mutants confirmed that they are both allelic to DaPKC (Tania Ferreira unpublished results). We denominated them *aPKC*^{TS} and *aPKC*^{PB1}.

Table. 2 - Complementation analysis of *aPKC* alleles

	aPKC*^{TS}*/Cyo	***aPKC*^{PB1}*/Cyo***	***aPKC*^{K06403}*/Cyo***	**DF6482/Cyo**
aPKC*^{TS}*/Cyo	Lethal*	Sterile (Cyo^{+})	Sterile (Cyo^{+})	Sterile (Cyo^{+})
aPKC*^{PB1}*/Cyo	Sterile (Cyo^{+})	lethal	lethal	lethal
aPKC*^{K06403}*/Cyo	Sterile (Cyo^{+})	lethal	lethal	lethal
DF6482/Cyo	Sterile (Cyo^{+})	lethal	lethal	lethal

*Lethality is most likely due to a second-hit lethal mutation.

2. Maternal phenotype

As referred above, the 2 novel aPKC alleles were selected in a maternal mutant screen for defects in embryonic soma and cuticle formation. We therefore decided to investigate which were the maternal defects underlying these phenotypes. In embryos with maternal contribution of *aPKC*^{TS}/DF6482 and *aPKC*^{PB1}*GLC* maternal mutants, cellularization appears to be normal (Fig.10, compare B and C with A). As GBE proceeds during gastrulation, the ectoderm epithelium starts to lose integrity and same cells acquired a rounded shape (Fig.10, B',B'',C' and C'' compare with A' and A''). This observed maternal phenotype is reminiscent to the one described for the loss-of-function allele *aPKC*^{K06403} (Wodarz, Ramrath et al. 2000; Harris and Peifer 2007) (Fig.10, D and D').

Western blot analyses allowed us to confirm that both alleles are not protein null alleles (Fig.16, left assay)

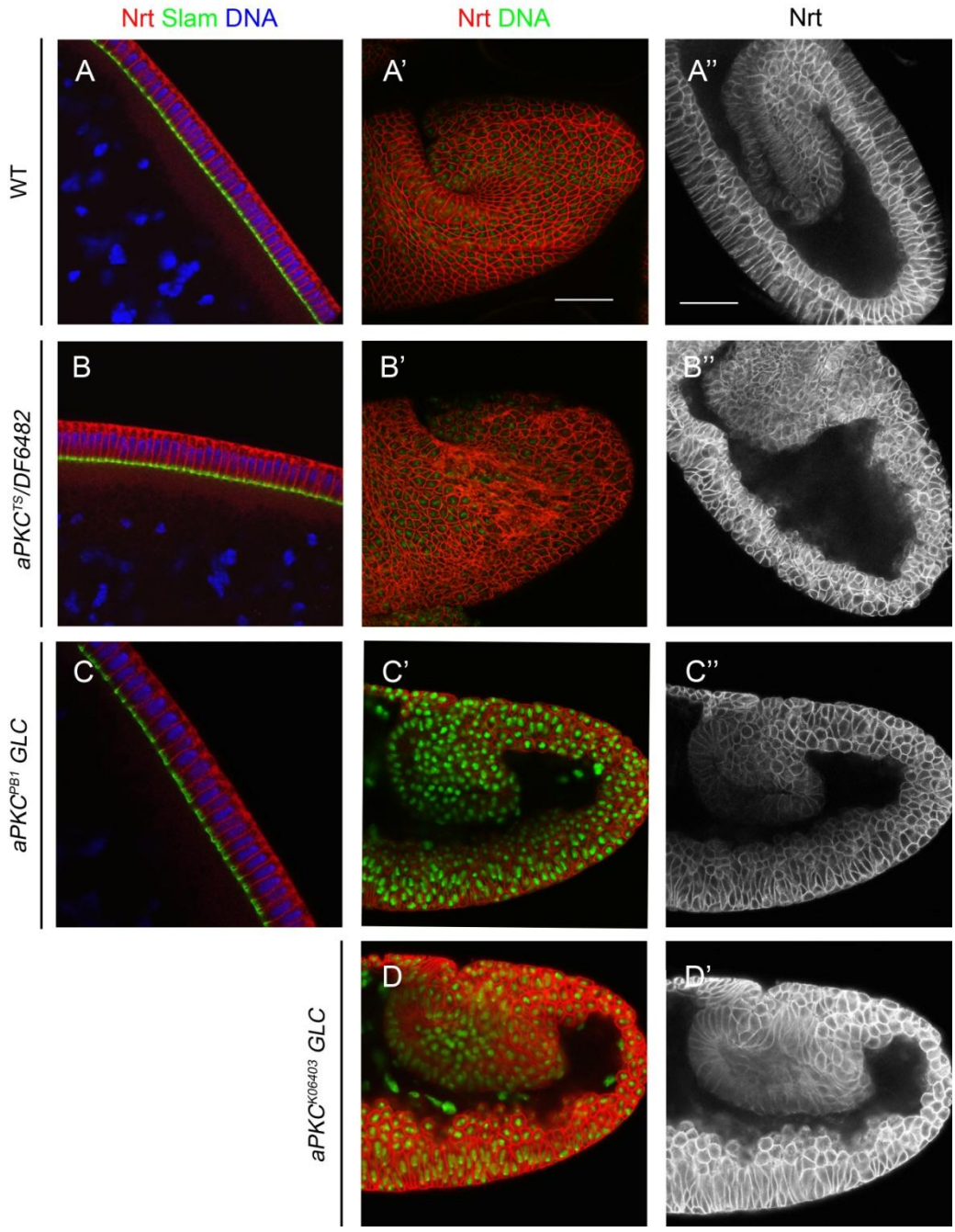

Fig. 10 - Loss of epithelial integrity during GBE in DaPKC maternal mutants. Cellularization is normal in both *aPKC*^{TS} (B) and *aPKC*^{PB1} (C) (Slam (green), Nrt (red) and DNA (blue)), when comparing with the WT (A). During GBE of aPKC maternal mutants the ectoderm cells appear to lose epithelial integrity and acquire a rounded shape (B', B'', C' and C'' comparing with A' and A''). This phenotype is reminiscent of what was published for the *aPKC*^{K06403} loss-of-function allele (E and E') stained for DNA (green in A', B' C' and D) and Nrt (red in A'', B'',C'' and D').

By immunostaining, we can detect aPKC protein in both maternal mutants. However while the protein is properly localized at the apical domain in *aPKC*^{TS} allele (Fig.11, A'') it is delocalized from the same domain in aPKC^{PB1} allele (Fig.11, B-B'').

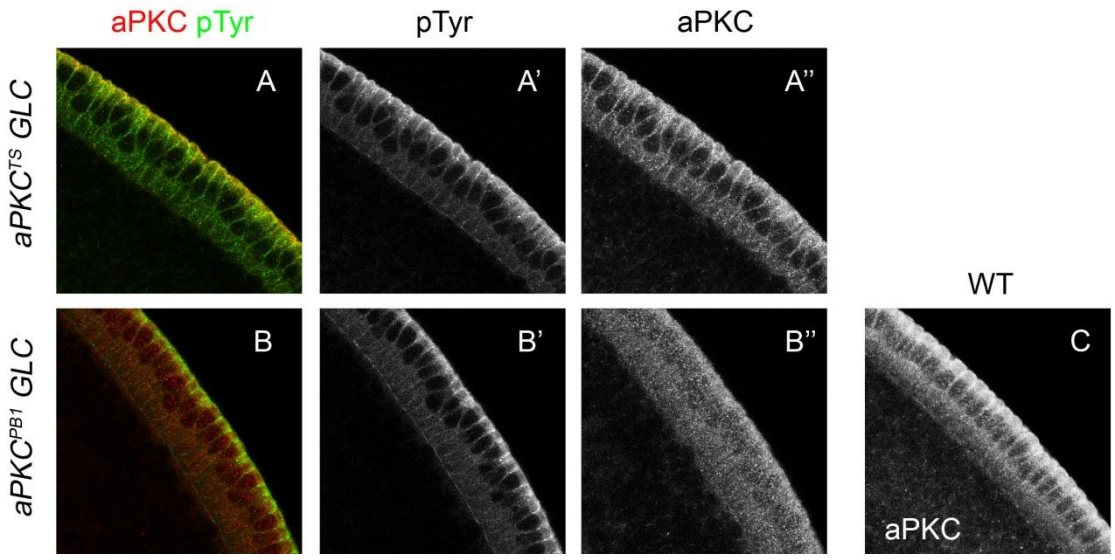

Fig. 11 - aPKC localizes in *aPKC*^{TS}*GCL* but not in *aPKC*^{PB1}*GLC*. Sagital sections from the ventral side of the embryo ectoderm at late stage 5. aPKC protein is present in both aPKC maternal mutants and is apically localized at the cortex of *aPKC*^{TS} maternal mutant cell (A and A''), and in the WT embryo (C), but in aPKC^{PB1} (B and B'') the aPKC protein is diffused and is not enriched at apical cortex of the cells. Membrane was labeled using pTyr.

3. Aggregates formation during early Germ Band Extension

We noticed that during early GBE in *aPKC*^{TS} mutants, the apicaly located aPKC protein started to form aggregates close to the membrane (Fig.12, B-B' compare with A-A'). In *aPKC*^{PB1} GLC although the aPKC protein is not apical during this stage, it still forms the same later aggregates, like in *aPKC*^{K06403} GLC (Harris and Peifer 2007). To understand better the nature of these aggregates, we checked for the presence of several proteins known to interact with aPKC (Fig.12 C,C',E,E',G and G'). We show that aPKC, Baz and Par-6 colocalize with these aggregates (Fig.12 D,D',F,F',H and H'). We also observe the mislocalization of adherens junctions proteins like Armadilho (Fig.13, F-F'), and the accumulation of F-actin (Fig.13, E-E') within the aggregates.

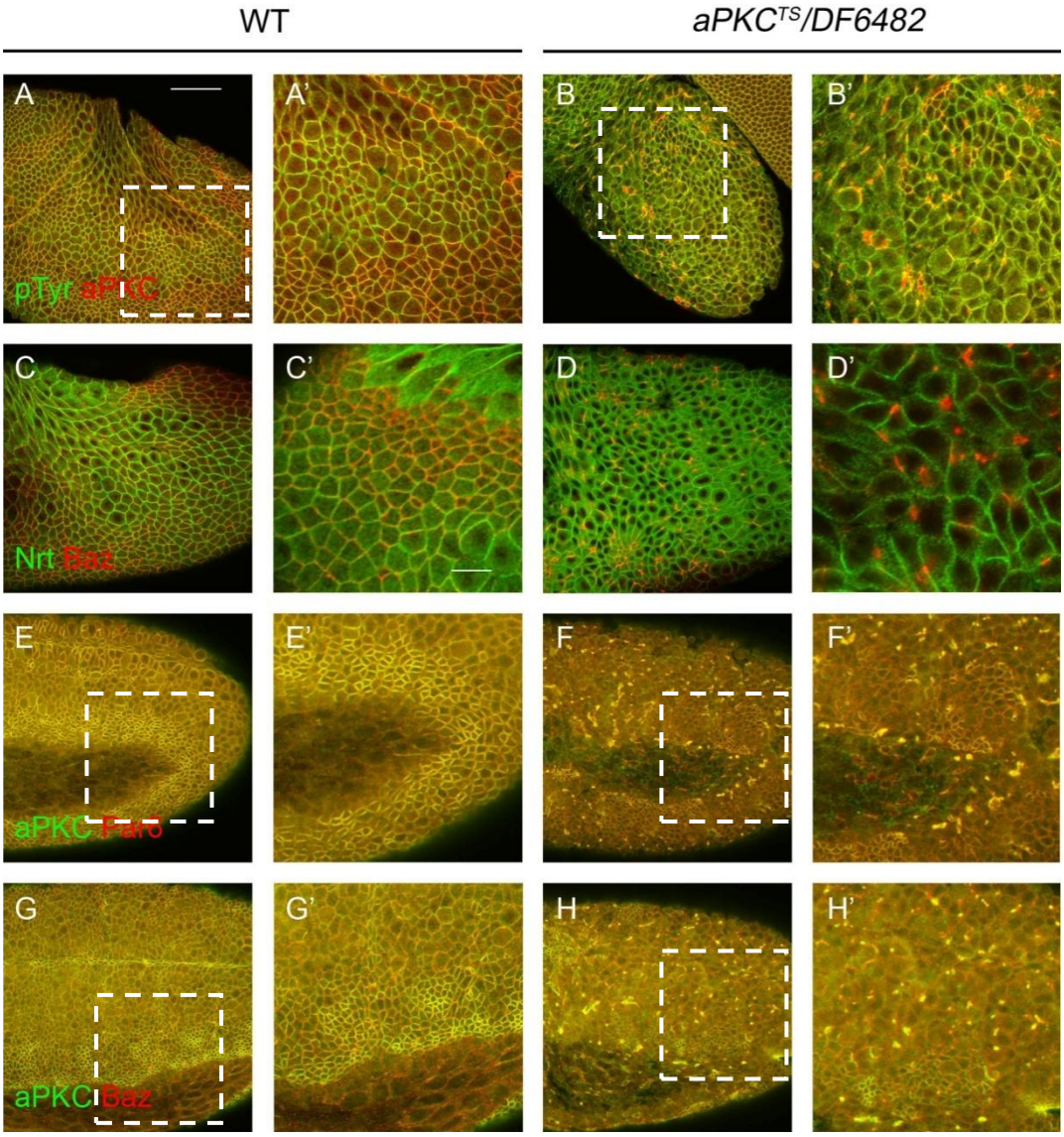

Fig. 12 – aPKC aggregates formation during GBE, contain Par6 and Baz. WT embryonic ectoderm cells are polygonal in shape (A, A', C, C') with a well defined apical cortex (C, E, G). In *aPKC^{TS}* maternal mutants some cells loose epithelial morphology and acquire a rounded shape (B, B' comparing to A, A'; and D, D' comparing to C, C'). In these mutants, the apical cortex is not properly organized (F compared to E and H compared to G). In WT cells, apical components are evenly distributed around the cell cortex (aPKC: E' and G'; Par6: E' and Baz: G') while in *aPKC^{TS}* these apical manners are clumped together in apical aggregates (F' comparing to E' and H' comparing to G'). (A, C, E, G) WT ventro-lateral ectoderm (stage9-10 embryo). (A', C', E', G') insets of the outline region in A, B, C and D, respectively. (B) *aPKC^{TS}* dorsal ectoderm (stage 9-10 embryo), (B') region outlined in B. (D, F, H) aPKC^{TS} ventro-lateral ectoderm (stage 9-10 embryo). (D', F', H') region outlined in D, F and H, respectively.

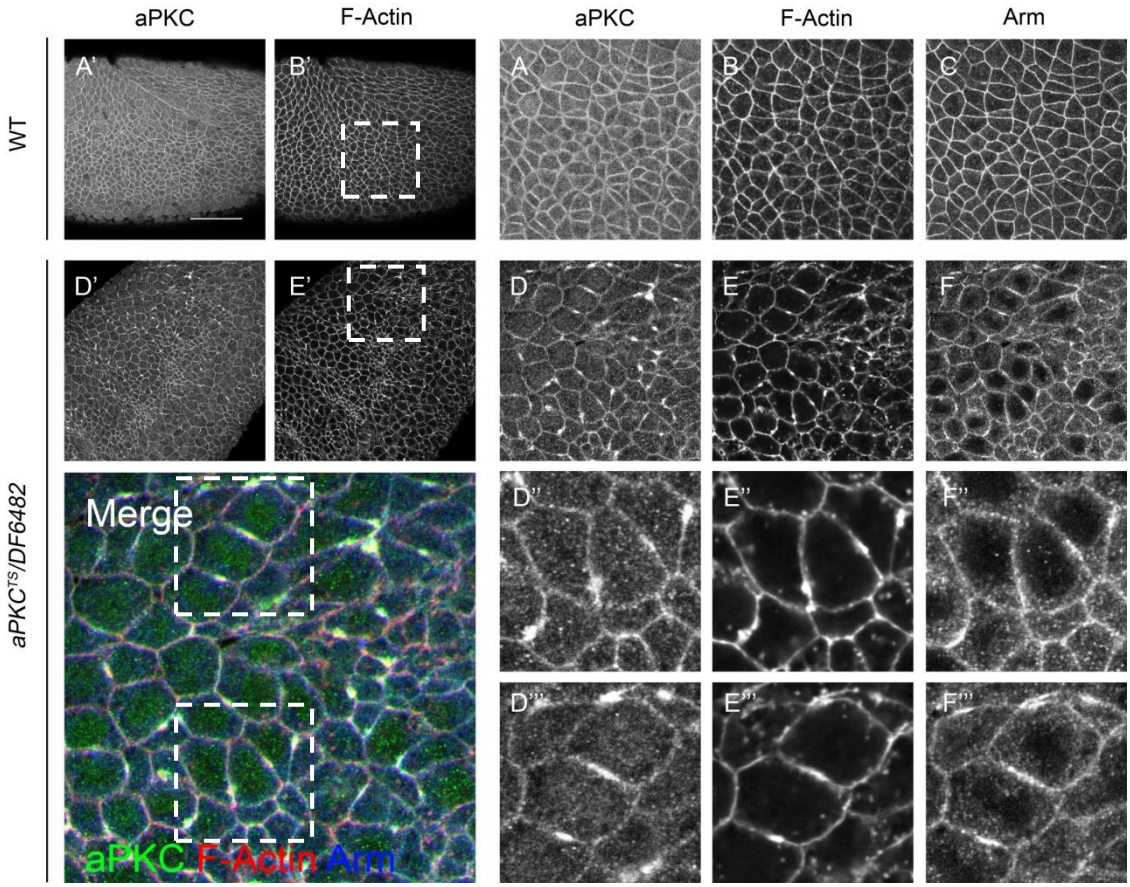

Fig. 13 – *aPKC* aggregates formation during GBE contain F-Actin and Arm. In WT embryos, *aPKC*(A, A'), F-actin (B, B') and Arm (C) are evenly distributed around the cell cortex. In $aPKC^{TS}$ maternal mutants ($aPKC^{TS}$/DF6482) distribution of these proteins is no longer homogeneous, but instead colocalizes in aggregates (aPKC (D', D, D'', D'''); F-actin (E', E, E'', E'''), Arm (F, F'', F''')) visible at the cell cortex. A', B', A, B, C: Dorso-lateral ectoderm in cut embryos (stage 7). D', E', D, E, F): ventro-lateral ectoderm of $aPKC^{TS}$ maternal mutants (stage 7). Merge panel: magnification of the area outlined in B'.D'', E'', F'': inset of the upper region outlined in merge panel. D''', E''', F''': inset of the lower region outlined in Merge panel.

4. $aPKC^{TS}$ allele is zygotic viable at 25ºC

The $aPKC^{TS}$/*DF6482* maternal mutants are 100% lethal at 25ºC (Graph. 1) (Tania Ferreira unpublished results), while $aPKC^{TS}$/*DF6482* zygotic mutants are 100% viable at 25ºC (Fig.14), probably due to the $aPKC^{WT}$ maternal contribution. Nevertheless, these females are sterile, their eggs do not hatch. However no $aPKC^{TS}/aPKC^{TS}$ flies can be retrieved, suggesting that there might be a lethal second hit mutation in the background of our $aPKC^{TS}$ allele. Since $aPKC^{TS}$/*DF6482* and $aPKC^{TS}$GLC have similar maternal phenotypes, we conclude that the lethal second hit in $aPKC^{TS}$ is not related to the observed phenotypes.

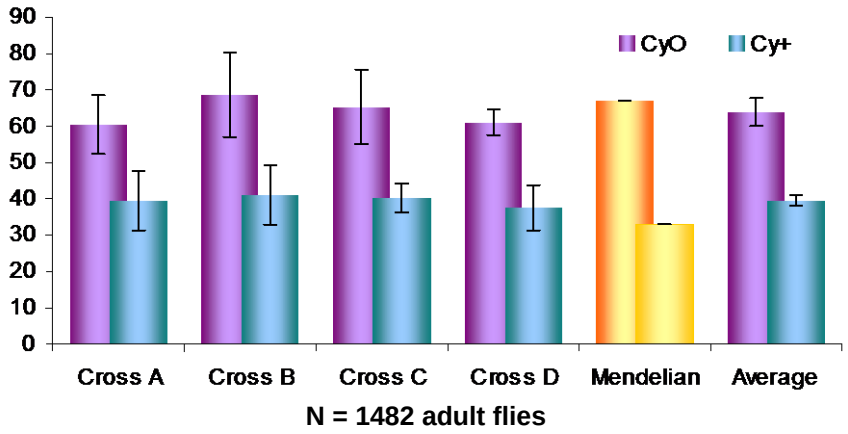

Graph. 1 - *aPKC^{TS}* allele does not affect zygotic viability at 25ºC. Zygotic mutants of *aPKC^{TS}* shows Mendelian segregation ratio (should be noticed that Cyo/ Cyo individuals are not viable). The progeny (F1) of four independent crosses (a*PKC^{TS}*/ Cyo x *DF6482*/ Cyo) were scored for Cy wings. Since Cy is a dominant marker, absence of curly wings means that the adult fly must be mutant for *aPKC^{TS}*. For each cross were generated three replicas. All graphs are shown with 95% intervals of confidence.

The *aPKC^{PB1}* maternal mutant are 100% lethal at 25ºC (Tania Ferreira unpublished results) and the zygotic mutants all die as 2nd instar larvae (100% zygotically lethal), like *aPKC^{K06403}* that is also 100% zygotic lethal (Table.2)

Fig. 14 – Zygotic *aPKC^{TS}/DF6482* mutants are viable. *aPKC^{TS}/DF6482* zygotic mutants are 100% viable at 25ºC (middle panel). The ecloded adults don't have any obvious phenotypes, besides sterility. Left panel: detail of the eye; right panel: detail of the wing.

5. *aPKC^{TS}* phenotype is Temperature-Sensitive

Table. 3 – Zygotic viability of *aPKC^{TS}* allele is affected by temperature. For these analyses the progeny (F1) of six independent crosses made at temperatures described on the table (*aPKC^{TS}*/ Cyo x *DF6482*/ Cyo) were scored for Cy wings. Since Cy is a dominant marker, absence of curly wings means that the adult fly must be mutant for *aPKC^{TS}*.

	25ºC		**27-28ºC**		**30ºC**	
aPKC^{TS}/DF6482	38%	37%	38%	27%	0%	0%
aPKC^{TS}/CyO ***CyO/+***	62%	63%	62%	73%	100%	100%
Adult flies (n)	89	104	89	194	37	45

As referred above, *aPKC^{TS}/DF6482* zygotic mutants are 100% viable at 25ºC. However, when subjected to an increase in temperature (30ºC) during the development this flies, do not eclode and are 100% lethal. This indicates that the *aPKC^{TS}* zygotic viability is temperature-sensitive (TS). Accordingly, intermediate temperatures (25ºC<T<30ºC) lead to intermediate phenotypes of zygotic viability. Viability reduces while increased temperature (data not shown). Additionally, all flies that hatch at these intermediate temperatures consistently show defects in abdominal dorsal closure (Fig.15).

Like zygotic viability and adult dorsal closure the wing blade epithelium also displays a TS phenotype. Cell death increase in the blade as temperature increases. It is also interesting that regardless of the temperature/cell death, we fail to detect phenotypes in the adult wing (Leonard Guilgur unpublished data).

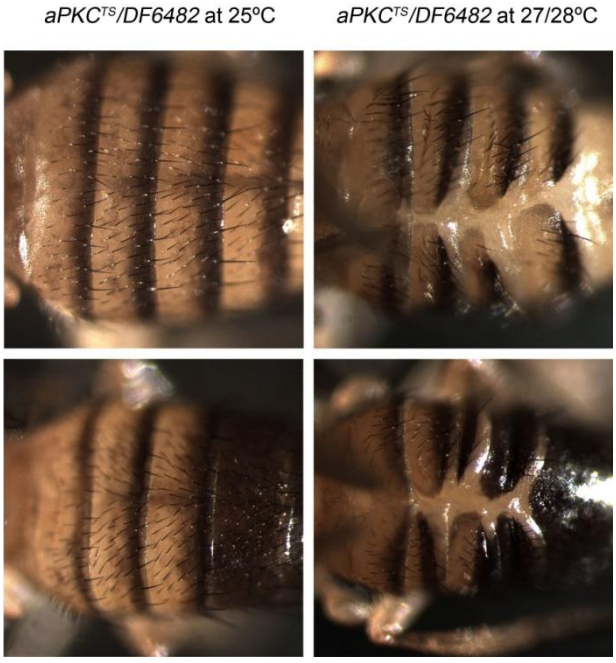

Fig. 15 - Zygotic mutant *aPKC^{TS}/DF6482* shows adult dorsal closure defects at semi-permissive temperatures. Adult fly ecloded at 27-28ºC (right column) and control at 25ºC (left column). Two examples of each case are represented here.

6. *aPKC^{TS}* mutation is within the kinase domain

Sequencing analyses of the *aPKC^{TS}* allele revealed a missense mutation within the kinase domain: aPKC F532L. Due to the nature of the aPKC^{TS} mutation and the observed TS behavior of the zygotic mutant phenotypes, we hypothesized that aPKC^{TS} is a kinase-TS.

We then analyzed if the *aPKC^{TS}* was being properly activated. As an approach we performed western blots analyses, to detect the presence of phosphorylated forms and the levels of aPKC on *aPKC^{TS} and aPKC^{PB1}*, by using as negative control the loss of function *aPKC^{K06403}*. The results indicate that both, activity and levels of aPKC are normal in *aPKC^{TS} and aPKC^{PB1}* alleles (Fig.16, right (phosphorylated form) left (levels)). Whereas *aPKC^{K06403}* show only a residual levels and no phosphorylated form.

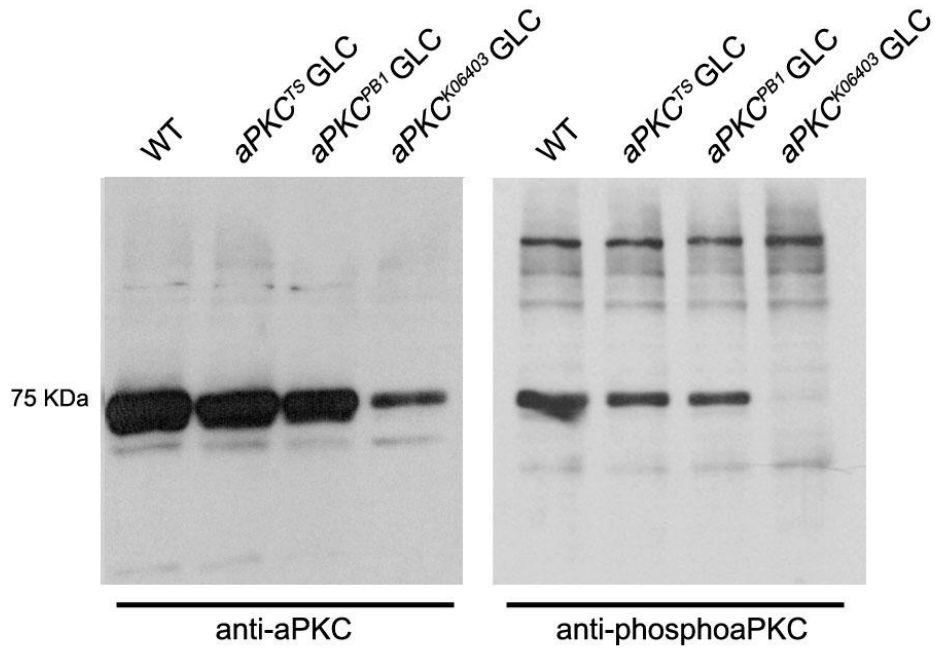

Fig. 16 – aPKC^{ts} and aPKC^{PB1} protein levels are similar to WT. Western blot detection of aPKC shows the same relative amount of protein in both *aPKC^{TS}* and *aPKC^{PB1}* GLC comparing with WT. *aPKC^{K06403}* described as a null allele shows residual levels of protein. Detection of the presumably active forms of aPKC (phosphorylated aPKC). *aPKC^{TS}* and *aPKC^{PB1}* Show comparable levels of phosphorylated aPKC as WT. In *aPKC^{K06403}* the phosphorilated aPKC is absent.

We confirmed these results using a technique in which there is a specific delay in the rate of migration of phosphorylated proteins in relation with non phosphorylated forms in SDS-PAGE. Results for *aPKC^{TS}/DF6482* shows that, the levels of the presumable phosphorylated form of aPKC (Fig.17, asterisk), does not differ from those in the control. Although we still need to perform a phosphatase treatment, and analyze the negative control *aPKC^{K06403}*, to be sure about the specificity of these results.

Concerning the other allele, *aPKC^{PB1}*, it has a mutation in the PB1 domain (D77N). This residue is highly conserved and is placed within acidic regions of PB1. This region is involved in the formation of salt bridges necessary for the aPKC-Par6 interaction (Fig. 26 of Discussion) (Hirano, Yoshinaga et al. 2005).

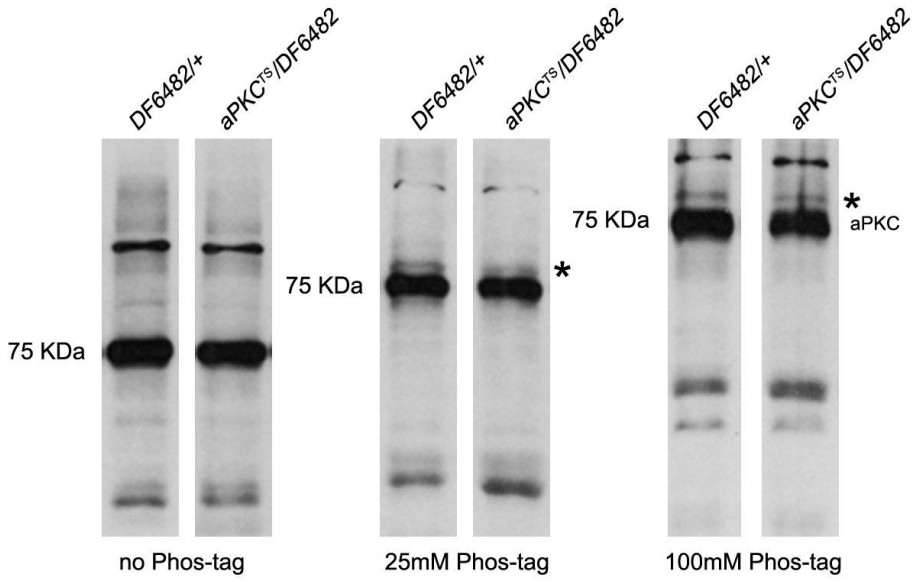

Fig. 17 - Phosphorylated aPKC levels in *aPKC^{TS}* mutants are similar to WT. Western blot showing that, when no phos-tag is added the phosphorylated proteins are covered by the unphosphorylated ones, (compare left panel with middle and right panels). Phos-tag treatment delays migration of the presumably phosporylated forms of aPKC (asterisk).

7. *aPKC^{TS}* mutant protein interact in vitro with Par6

To better understand the mechanisms intrinsic to this allele, we created several UAS lines for aPKC tagged with GFP or Myc, both N-terminal and C-terminal. These lines were tested under control of the ubiquitous Actin-Gal4 driver. However, we failed to retrieve a functional line, since all showed an abnormal localization of the GFP signal in follicle cells (fig. 18, A).

Fortunately, we acquired a functional Par6-GFP from Jeniffer Zallen (unpublished results) allowed us to pursuit this analyzes. The Par6-GFP line is under an endogenous promoter and is expressed in a *Par6$^{\Delta 226}$* loss of function mutant background. This means that all the functional Par6 protein is the one associated with the GFP tag. Moreover, this shows to be functional, since it is apically localized in follicle cells. Additionally, in the *aPKC^{TS}/DF6482* mutant background, it shows the expected phenotype for the follicle epithelium (fig. 18, B and C)

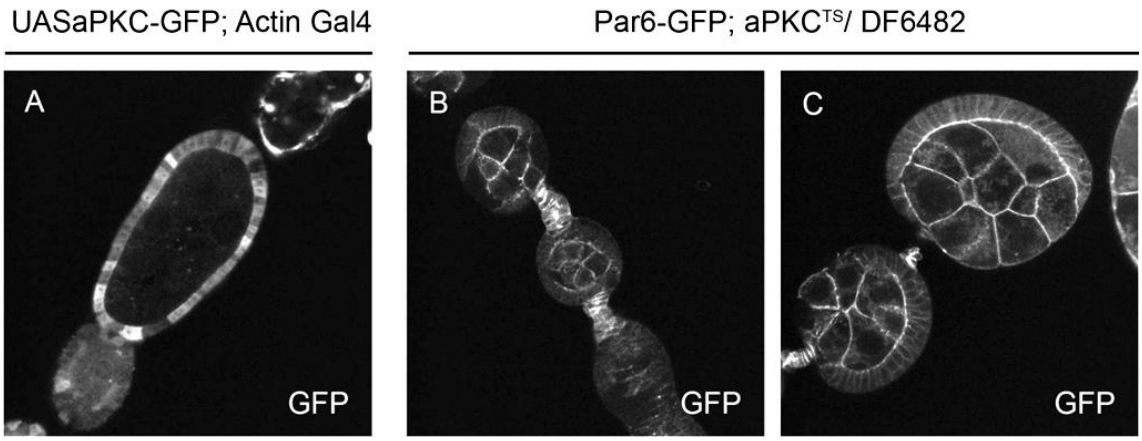

Fig. 18 – PARG-GFP is functional and localizes properly to the apical domain of follicle cells. UAS aPKC-GFP (N-terminal) line under the expression of the ubiquitous Actin Gal4 driver, showing the abnormal localization of the tagged aPKC-GFP protein (A). Par6-GFP expression is under the control of its endogenous promoter, in Par6$^{\Delta 226}$ and *aPKC^{TS}/DF6482* mutant background, showing proper apical localization of the Par6-GFP protein (B and C).

Knowing that Par6 is a binding, we decide to investigate if it could interact with aPKC^{TS}. This would allow us to overcome the difficulties in generating the UAS aPKC lines, and be able to immunoprecipitate aPKC^{TS} and (indirectly) its other binding partners.

We immunoprecipitated protein extracts from Par6-GFP*Par6$^{\Delta 226}$*; *aPKC^{TS}/DF6482* mutant and as a control from Par6-GFP; *DF6482/+*. This assay allowed us to confirm that both aPKC^{WT} and aPKC^{TS} interact with Par6-GFP *in vitro* (Fig. 19) Meaning that aPKC^{TS} mutation does not affect aPKC interaction with Par6.

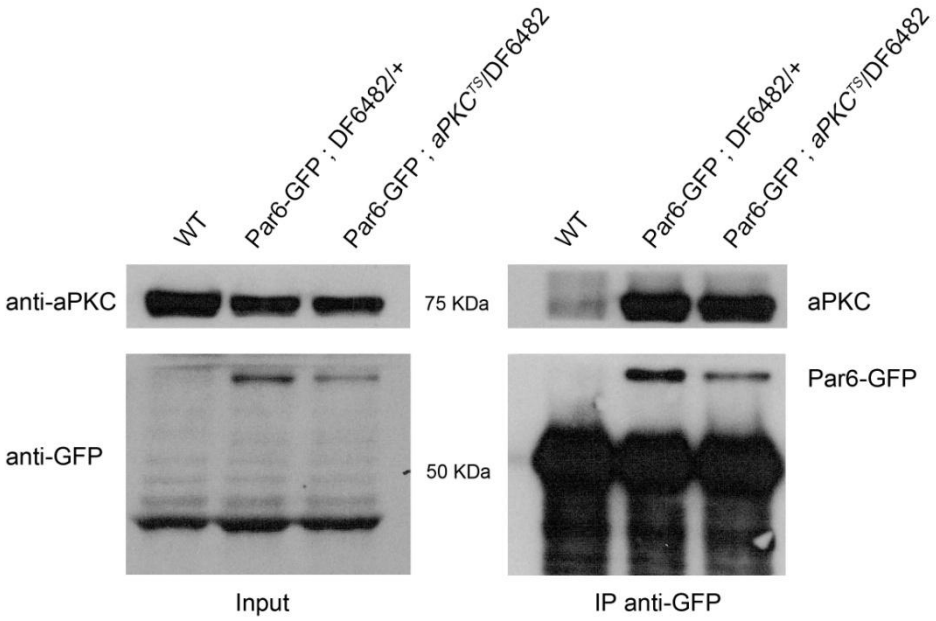

Fig. 19 – *aPKC^{TS}* interacts with Par6. The left panel represents the protein extract equivalent to the one used for the IP (input). The upper left panel indicates the levels of aPKC protein in all input samples, and the lower left panel relates to the Par6-GFP. aPKC is detected an all samples, but Par6-GFP is not detected in the WT extract (left column, control). The right panel represents the result from the IP (output). The lower right panel shows Par6-GFP detection an all samples, except the WT. Upper right panel shows *aPKC^{TS}* (middle column) and *aPKC^{TS}* (right column) being specifically immunoprecipitated by Par6-GFP. In the absence of Par6-GFP (left column, control) *aPKC^{WT}* is not immunoprecipitated.

8. *aPKC^{TS}* follicle cells clones are normal at 25ºC

As previously referred, the zygotic phenotype of aPKC^{TS} are temperature sensitive. It has been proposed a role for aPKC in oogenesis, independent of its kinase activity (Kim, Gailite et al. 2009). Since we hypothesize that the aPKC^{TS} allele is a kinase-TS, we decided to investigate the zygotic phenotypes during oogenesis.

aPKC^{TS} mutant clones show no phenotype at 25ºC (Fig. 20, marked between arrowhead heads in A-A''). Cell morphology, apical localization of aPKC and Arm in *aPKC^{TS}* mutant clones are comparable to WT (Fig. 20, marked between arrowhead heads in B-B'').

aPKC^{PB1} phenotypes are independent of temperature and recapitulate what has been published for *aPKC^{K06403}* (Kim, Gailite et al. 2009). As expected, in *aPKC^{PB1}* mutant clones the cells are rounded and multilayered (Fig. 20, C-C''), while what sometimes seems to be an invasive behavior (Fig. 20, arrowhead head D-D'', *aPKC^{PB1}* mutant cells

invade the space between WT follicle cell and germ line). Additionally, both aPKC and Arm proteins are delocalized from apical domain (Fig. 20, D-D').

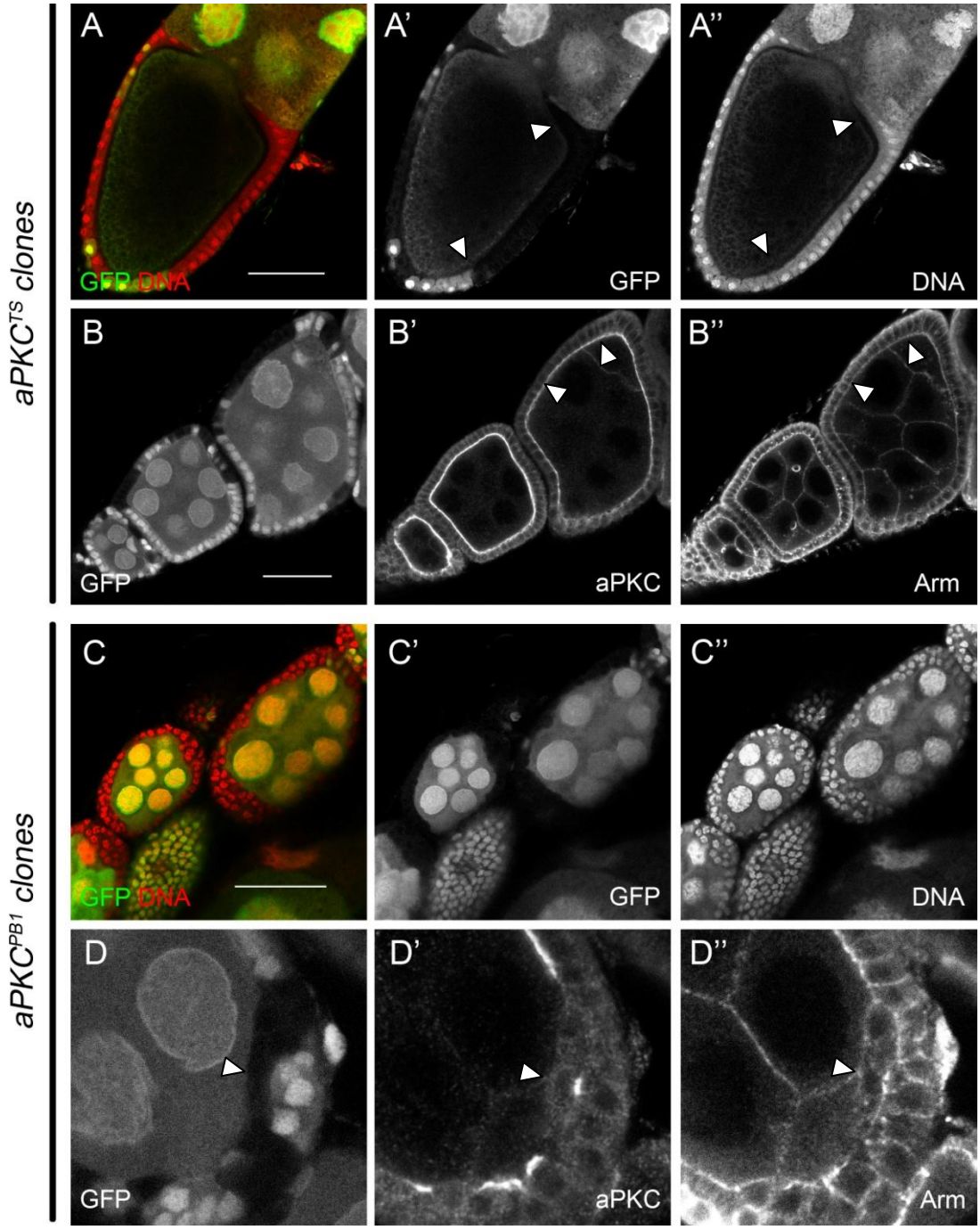

Fig. 20 – Follicular epithelium is normal in *aPKC^{TS}* mutant clones at 25ºC, whereas *aPKC^{PB1}* is multilayered. aPKCTS mutant clones (aPKCTS/aPKCTS) are comparable to WT at 25ºC (A, A', A''). Nuclear positioning (A, A', A''), APKC localization (B') and Arm distribution (B'') are normal. aPKCPB1 mutant clones exhibit a multilayer organization (C-D'') and both aPKC and Arm proteins are displaced from the apical cell domain (D', D''). These mutant cells seems to be able to have an invasive behavior, occupying the space between the WT follicle cells and the germline (D-D'', arrowheads). In all pictures, homozygous mutant clones are marked by the absence of GFP. Scale bar: 50µm

9. *aPKC^{TS}* follicle cells clones at 30ºC and *aPKC^{TS}*/DF6842 show defects in encapsulation

Surprisingly, when analyzing *aPKC^{TS}/DF6482* ovaries we observed defects even at 25ºC, follicle epithelium does not surround completely the nurse cells (Fig. 21, C-E'). However follicle epithelium that remains shows a normal morphology, with aPKC and AJs components proper localized. The same phenotype is recapitulated by aPKC^{TS} homozygous mutant cells that underwent development at 30ºC (Fig. 21, A-B'''').

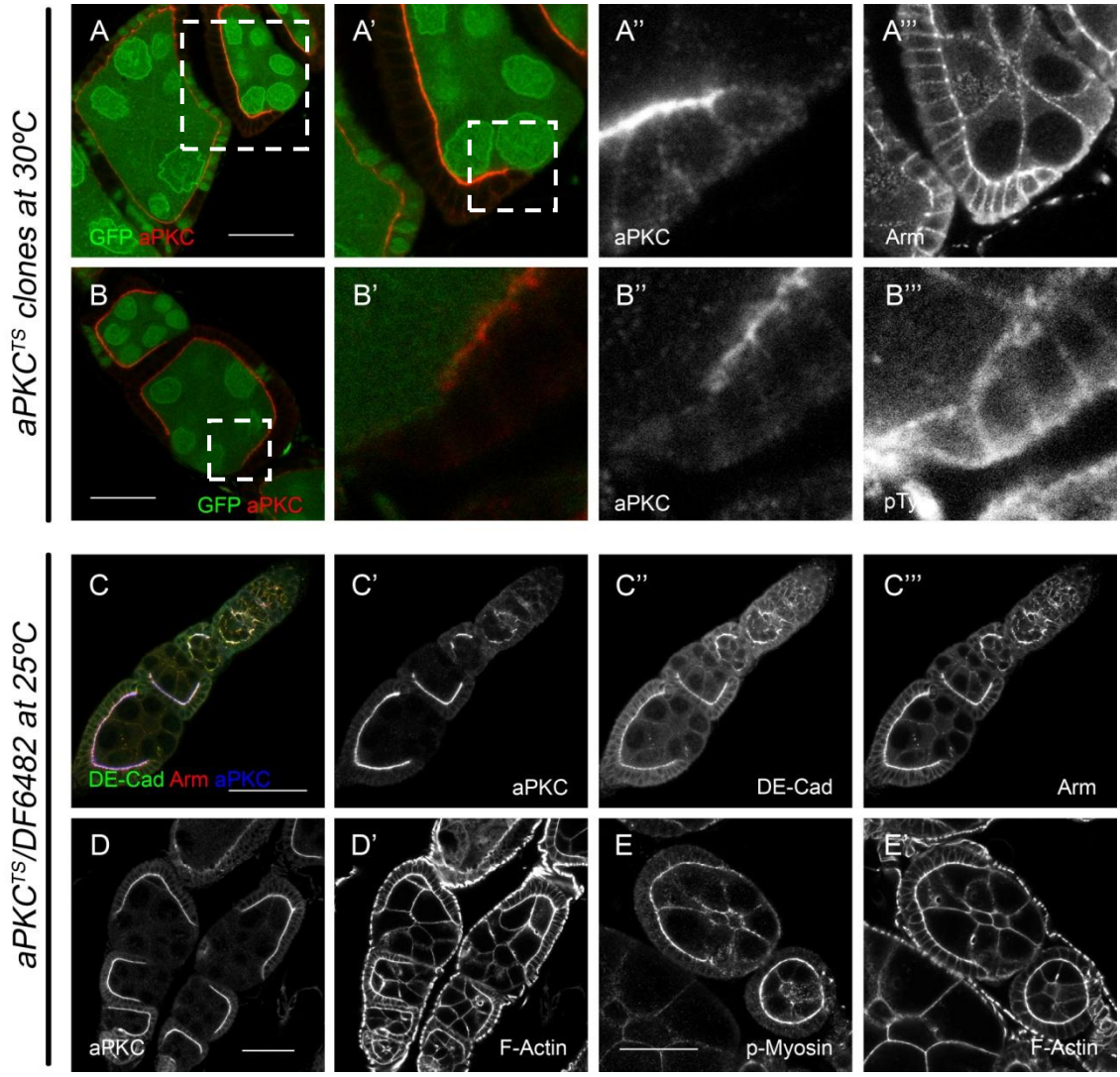

Fig. 21 – *aPKC^{TS}* mutants clones at 30ºC and *aPKC^{TS}/DF6482* show defects in Cyst encapsulatio. *aPKC^{TS}/DF6482* follicle cells are properly polarized (C-E') and AJs components are correctly positioned (C'', C'''). However, gaps can be observed with the follicular epithelium, which fails to enclose all the germline (C- C''', arrowheads). The same phenotype is observed for *aPKC^{TS}* homozygous mutant clones that developed under the restrictive temperature (30ºC) (A- B'''). Homozygous *aPKC^{TS}* mutant clones are marked by the absence of GFP.

To assess, if the observed defects were occurring early in follicular epithelium formation or latter as the epithelium matures and the egg chamber grows, we decide to analyze the germarium of aPKC^{TS} mutant flies (Fig. 22). We observed that the gaps defects started during follicular stage 1 (Fig. 22, arrowhead head A). DE-Cad and aPKC start to localize apically during stage 2b forming a continuing defined apical line. However is hard to analyze differences between *aPKC^{TS}/DF6482* mutant and control (*DF6482/+*) during stage 2b proteins localization (Fig. 22, arrow in A'', A''', B'' and B''').

This phenotype lead us to think if this fail start early during follicular epithelium formation. Because of that, we went to look into germarium. Here we found that defects in encapsulation starts It was observed that when follicular cell precursors make the mesenquimal to epithelial transition. At this stage it's hard to analyze differences between *aPKC^{TS}/DF6482* mutants and control (*DF6482/+*) localization (Fig. 22, arrow in A'',A''', B'' and B'''). However it's visible, that instead of forming a continuous and defined apical surface containing aPKC and DE-Cad surrounding the germ line like in control (Fig. 22 B), cells shows disorganized and some does not possess any polarization during follicle stage 1 (Fig. 22, arrowhead in A).

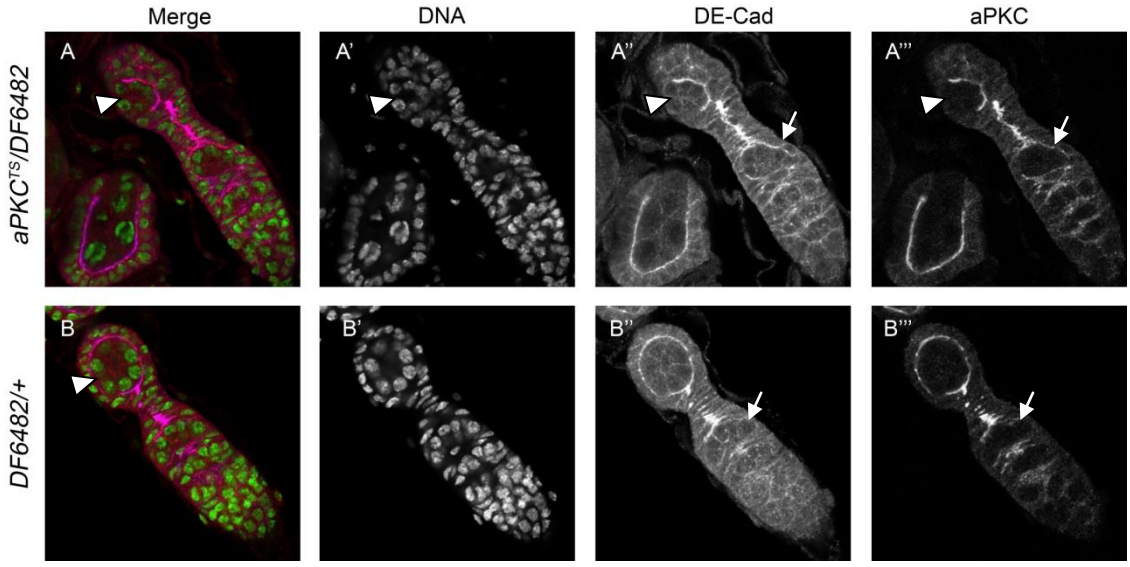

Fig. 22 – *aPKC^{TS}/DF6482* mutants fail to do MET dueing follicle epithelium formation. *aPKC^{TS}/DF6482* mutant cells fail to properly encapsulate the germline cells as soon as stage 1 in the germarium (A-A''', arrowhead). While in WT cells apical components accumulate continuously in the apical cortex of the cells (B-B'''), in *aPKC^{TS}/DF6482* cells this localization is discontinuous (A-A''', compare arrows with arrows in B-B''').